Arab J Sci Eng (2015) 40:1647–1655
DOI 10.1007/s13369-015-1623-z

RESEARCH ARTICLE - MECHANICAL ENGINEERING

Investigation on the Effects of Process Parameters on the Mechanical and Corrosion Behaviour of Friction Stir-Claded AZ31B Magnesium Alloy

K. Ganesa Balamurugan · K. Mahadevan

Received: 30 September 2014 / Accepted: 19 February 2015 / Published online: 13 March 2015

Abstract Al5086 aluminium alloy was claded to AZ31B magnesium alloy using friction stir processing. The effect of process parameters like tool rotational speed and travel speed on the corrosion resistance, microhardness and tensile properties of the claded AZ31B magnesium alloy was investigated. The study revealed that the samples processed at a higher process parameter range exhibited higher corrosion rate due to the presence of the higher percentage of magnesium trace elements on their surfaces. The precipitation of intermetallics in the stir zone influenced the microhardness values, and the intensity of intermetallics along the line determined the tensile properties of the claded AZ31B magnesium alloy.

Keywords Friction stir processing · AZ31B alloy · Al5086 alloy · Corrosion rate · Intermetallics

1 Introduction

Magnesium alloys are the most amenable materials in the transportation industries due to their low density. However, their wide ranges of applications have been limited by their poor corrosion resistance properties [1–3]. Various coating techniques like electrochemical coating, anodizing, thermal spraying, laser cladding, magnetron sputtering, plasma transferred arc process, tungsten inert gas method, are available to protect the metals from corrosive attacks [4–10]. However, defects such as pores and cracks are usually unavoidable in coatings [11–13]. Similarly, chemical conversion coatings are toxic and cause irritation and environmental hazards [14–17]. In the case of thermal spraying techniques, the kinetic energy of thermally sprayed particles is low and their thermal energy is high, due to which the defects such as pores and cracks are inevitable [18]. Mechanical cladding techniques like roll bonding and explosion cladding too have some limitations. In the case of explosion cladding, safer work area is needed, and it is suitable only for bulk material cladding. Accumulative roll bonding on Mg/Al system is normally carried out at elevated temperature, resulting in larger grain growth and the formation of massively cracked Mg/Al intermetallic compounds at the Mg/Al interface that leads to deterioration of mechanical properties [19]. Therefore, there is a need for a suitable cladding technique to overcome the above-mentioned limitations. The present work has attempted the friction stir processing as a cladding technique, and this has not been attempted before. The friction stir processing (FSP) is a solid-state processing technique that combines frictional heating and stirring motion to soften and mix the interface between two metal sheets [20–22]. The objective of the present work is to study the suitability of friction stir processing as a metal cladding technique to clad marine grade Al5086 aluminium alloy over AZ31B magnesium alloy. The effects of FSP process parameters on the mechanical and corrosion properties of the claded plates have been investigated to validate the suitability of the FSP as a cladding technique.

2 Experimental

Commercially available AZ31B magnesium alloy and marine grade Al5086 aluminium alloy plates were utilized in this

K. G. Balamurugan (✉)
Adhoc Faculty, Production Engineering Department,
National Institute of Technology, Tiruchirappalli 620015,
Tamil Nadu, India
e-mail: gbmpondy@gmail.com

K. Mahadevan
Mechanical Engineering Department, Pondicherry Engineering College, Pondicherry 605014, India

Fig. 1 Concave shoulder FSP tool with straight flutes

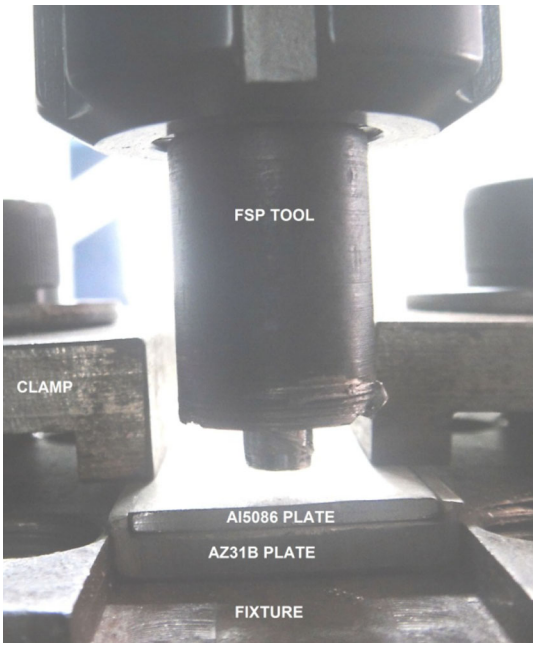

Fig. 2 Experimental set-up

research work. The substrate material was AZ31B magnesium alloy plate, and the clad material was Al5086 aluminium plate. The sample size of the magnesium alloy plate was 40 × 100 × 6 mm, and the sample size of the Al5086 aluminium alloy plate was 37 × 100 × 2 mm. A groove of 38 × 100 × 1.5 mm was machined out in the AZ31B substrate to accommodate the Al5086 clad plate to provide proper contact between the two plates. A CNC vertical milling centre was used to perform the friction stir cladding on the plates. A concave shoulder tool of 18 mm shoulder diameter, 5 mm pin diameter and 3.5 mm pin length with straight flutes was used for this purpose as shown in Fig. 1. HCHCr grade steel was selected as tool material and that was hardened to 58 HRC. The experimental set-up is shown in Fig. 2. After the activation of the preset program in the CNC machining centre, the tool performed the friction stir cladding operation on the plates. Two parallel passes were performed by taking 5 mm offset from the previous pass. A constant tool depth of 4.2 mm was maintained throughout the process. The process parameter values are shown in Table 1. The processed specimens

Table 1 Process parameters and their values

Tool rotational speed (rpm)				Tool travel speed (mm/min)	
500	710	850	1000	14	20

Table 2 Corrosion rates of claded samples

Combination no.	Tool rotational speed (rpm)	Tool travel speed (mm/min)	Corrosion rate (mm/year)
1	500	14	8.27E−07
2	500	20	1.52E−06
3	710	14	1.10E−06
4	710	20	9.70E−06
5	850	14	1.75E−06
6	850	20	1.86E−06
7	1000	14	0.000286
8	1000	20	0.003522

were subjected to tensile testing, microhardness testing and potentiodynamic polarization type of cyclic corrosion testing. The tensile test samples were machined out along the processed direction. The tensile test was carried out with the strain rate of 2.5 mm/min in a 5-ton machine. The microhardness samples were prepared from the stir zone of the claded AZ31B plates. Cut-out samples were mounted in a Bakelite moulding and polished to mirror finish. The constant load of 500 gf was applied on the stir zone with 10-s dwell time. For the corrosion tests, the sample size of 20 × 20 × 6 mm was cut from the processed surfaces and polished to mirror finish. The exposing area of the sample to the electrolyte was 1 cm^2. The testing range of potential was between −600 and +600 mV. The sweep rate was maintained as 300 mV/min. The electrolyte was 3.5 % NaCl solution. A platinum wire was kept as counter electrode, and the standard calomel was kept as a reference electrode.

3 Results

3.1 Corrosion Rate

The corrosion rates of Al5086 aluminium-claded AZ31B magnesium plates at different process parameter combinations are shown in Table 2.

The claded sample processed in combination 1 has a lower corrosion rate than the remaining combinations. Likewise, the samples processed in combination 2 have a higher corrosion rate than the other samples. From the observation, the corrosion rates of the claded samples have increased with an increase in rotational speeds and travel speeds. Moreover,

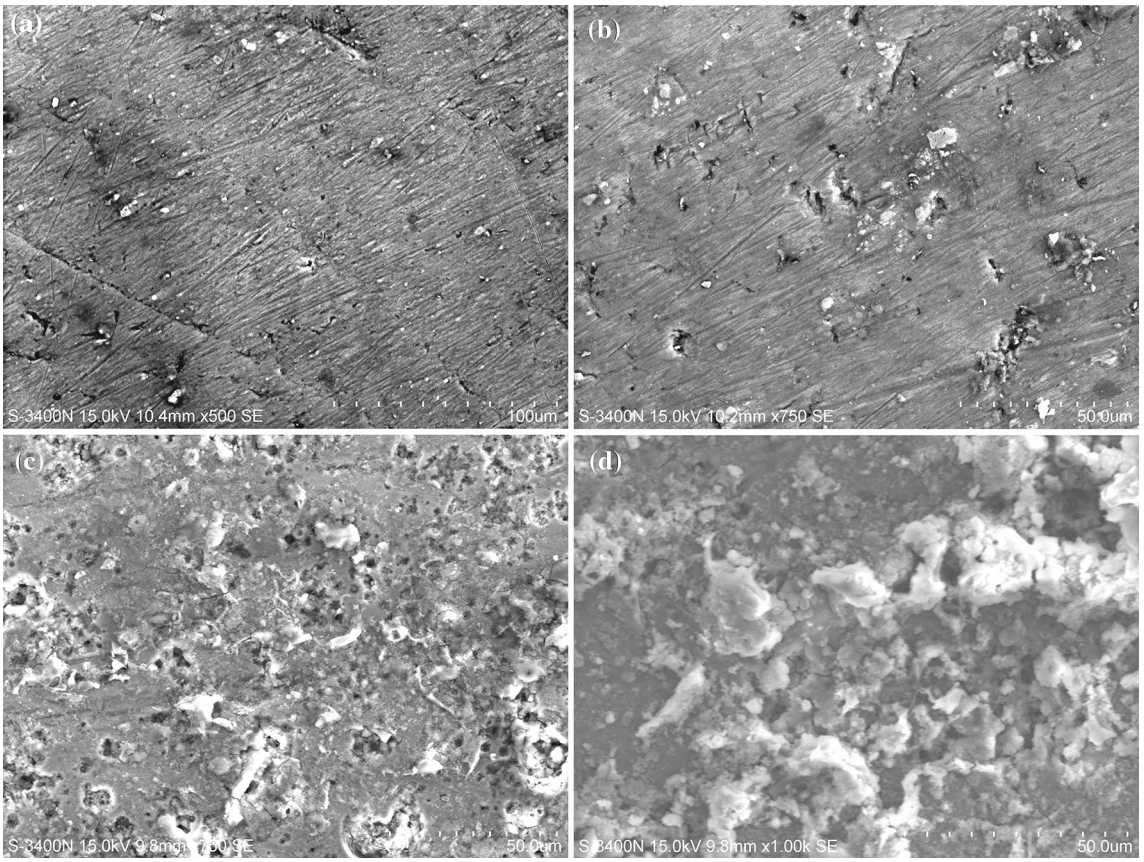

Fig. 3 SEM images of the corroded surfaces of Al5086-cladded AZ31B magnesium alloys processed at **a** 500 rpm—14 mm/min; **b** 500 rpm—20 mm/min; **c** 1000 rpm—14 mm/min and **d** 1000 rpm—20 mm/min combinations

the corrosion rates increased with an increase in tool travel speed compared to incrementing the tool rotational speed.

The corroded surface of cladded AZ31B magnesium plate processed in combination 01 (Fig. 3a) exhibits negligible salt precipitates and corrosion pits. However, the corroded surface of cladded AZ31B magnesium plate processed in combination 2 shows a few corrosion pits and salt precipitates (refer Fig. 3b). The corroded surfaces of cladded AZ31B magnesium plates processed in combination 7 (Fig. 3c) and combination 8 (Fig. 3d) were severely affected by salt precipitates and corrosion pits that were uniformly distributed along the surfaces. The surface of the sample processed in combination 8 has severe damages due to corrosion than the samples processed in combination 7.

3.2 Microhardness

The microhardness values of the Al5086-cladded AZ31B magnesium plates are listed in Table 3. The samples processed in 14-mm/min tool travel speed have higher microhardness values than the samples processed in 20-mm/min tool travel speed. However, exceptionally, the sample processed in combination 8 has higher microhardness than the sample processed in combination 7.

Table 3 Microhardness values of claded AZ31B alloys

Combination no.	Rotational speed (rpm)	Travel speed (mm/min)	Microhardness (Hv)
1	500	14	81
2	500	20	78
3	710	14	85
4	710	20	81
5	850	14	90
6	850	20	85
7	1000	14	82
8	1000	20	94

3.3 Tensile Strength

The tensile strengths of Al5086-cladded AZ31B magnesium plates are listed in Table 4. The samples processed in 14-mm/min tool travel speed have higher tensile strength than the samples processed in 20-mm/min tool travel speed.

Table 4 Tensile strength values of cladded AZ31B alloys

Combination no.	Rotational speed (rpm)	Travel speed (mm/min)	Tensile strength (MPa)
1	500	14	236
2	500	20	205
3	710	14	215
4	710	20	185
5	850	14	181
6	850	20	177
7	1000	14	166
8	1000	20	142

4 Discussion

4.1 Effect of Process Parameters on the Corrosion Rate of Claded Alloys

The Al5086-cladded AZ31B magnesium plates processed in higher process parameter ranges have higher corrosion rate. Among them, the samples processed in higher tool travel speed ranges show higher corrosion rates than the samples processed in higher rotational speeds. During friction stir cladding process, the pin of the FSP tool deforms the substrate AZ31B magnesium material and the cladded Al5086

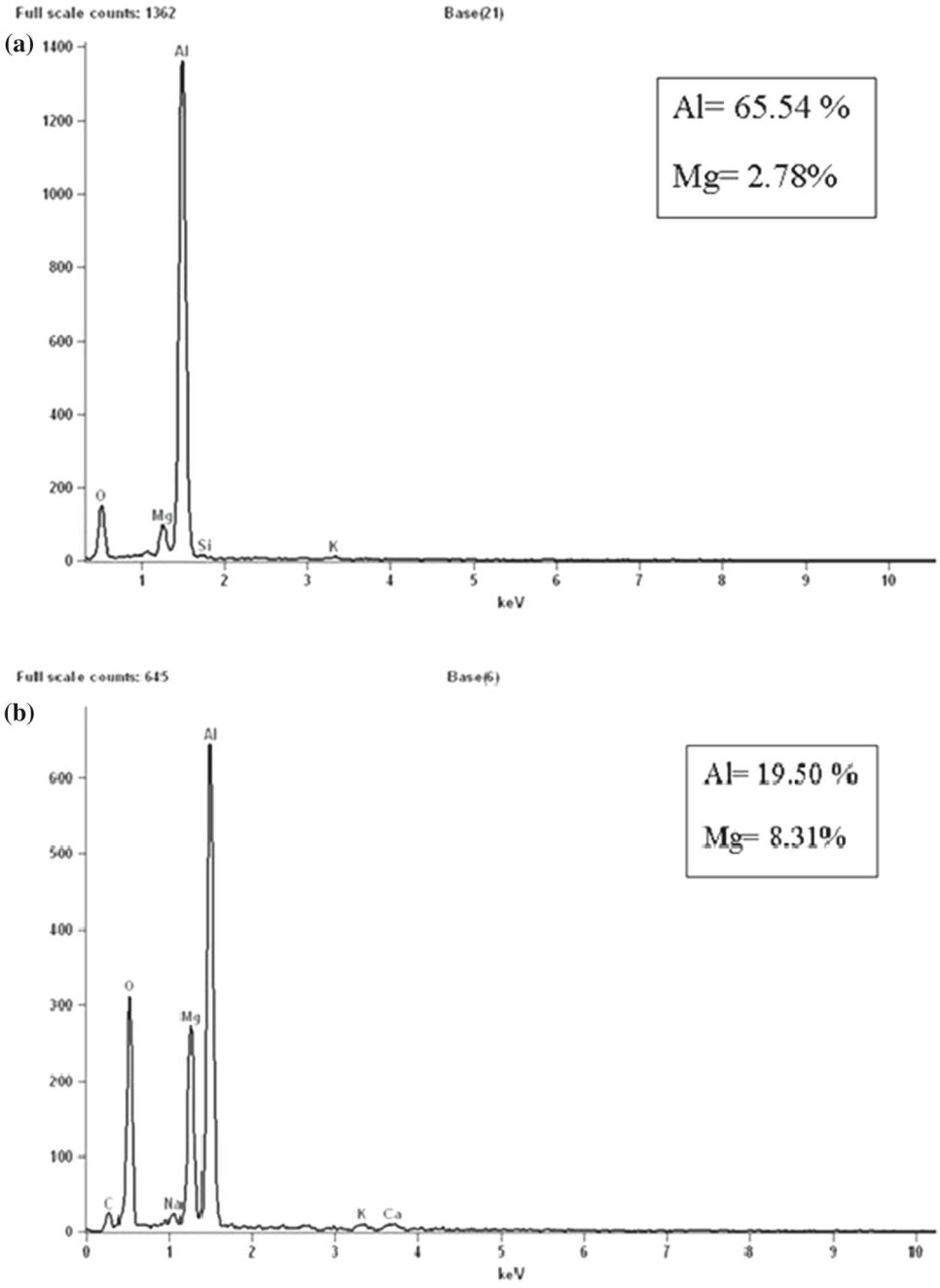

Fig. 4 Percentage of magnesium content of Al5086-cladded AZ31B alloy processed at **a** 500 rpm—14 mm/min, **b** 1000 rpm—20 mm/min

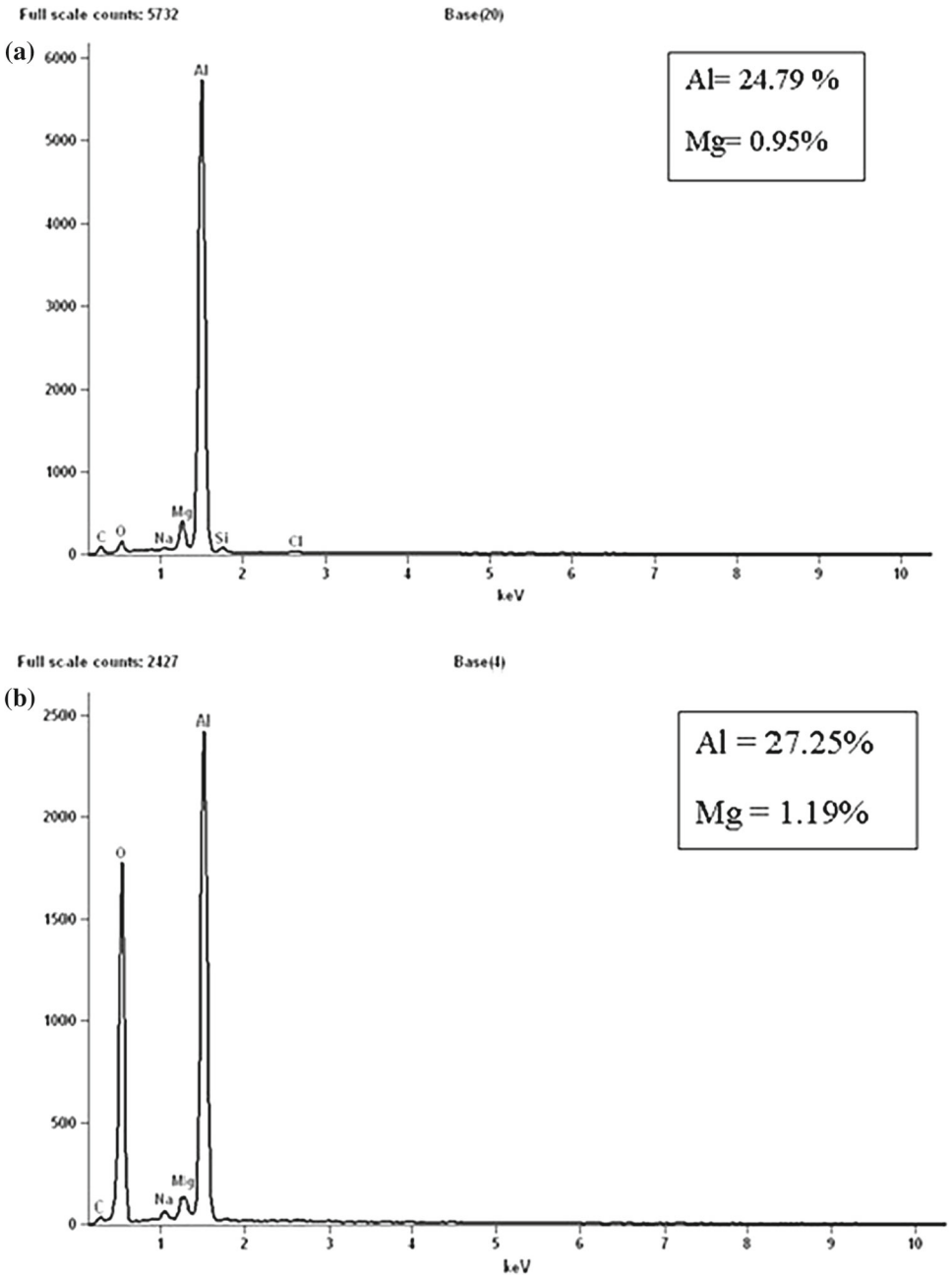

Fig. 5 Percentage of magnesium content in corroded samples of **a** 500 rpm—14 mm/min, **b** 1000 rpm—20 mm/min

aluminium material. The deformed metals expelled to the surface of the cladded aluminium alloy surface. The shoulder of the FSP tool confined the deformed materials and pasted them over the tool travelling path. Thus, during this process, the deformed substrate magnesium materials fused with the cladding aluminium alloy in the joint interface and some traces settled on the surface of the cladded plates. EDX results of the cladded samples processed in combination 1 and combination 8 are shown in Fig. 4. Figure 4a shows the magnesium percentage in the cladded surface of the sample processed in combination 1, and Fig. 4b shows the magnesium percentage in the cladded surface of sample processed in combination 8. The cladded sample surface of combination 1 has lower magnesium percentage compared to the cladded sample surface of combination 8. Higher ranges of rotational speed and travel speed are responsible for the increase in the magnesium elemental percentage on the surfaces of the cladded samples. High rotational speed ranges increased the frictional heat and resulted in large material deformation. Moreover, during high tool transverse movement, the ploughing action of the tool ploughed out more deformed materials to the surface. Due to less processing time, the ploughed-out materials settled on the surfaces of the cladded materials. During corrosion tests, magnesium traces on the surface of the cladded plates acted as sacrificial anodic centres and vanished quickly. Figure 5 shows the EDX results of the corroded cladded sam-

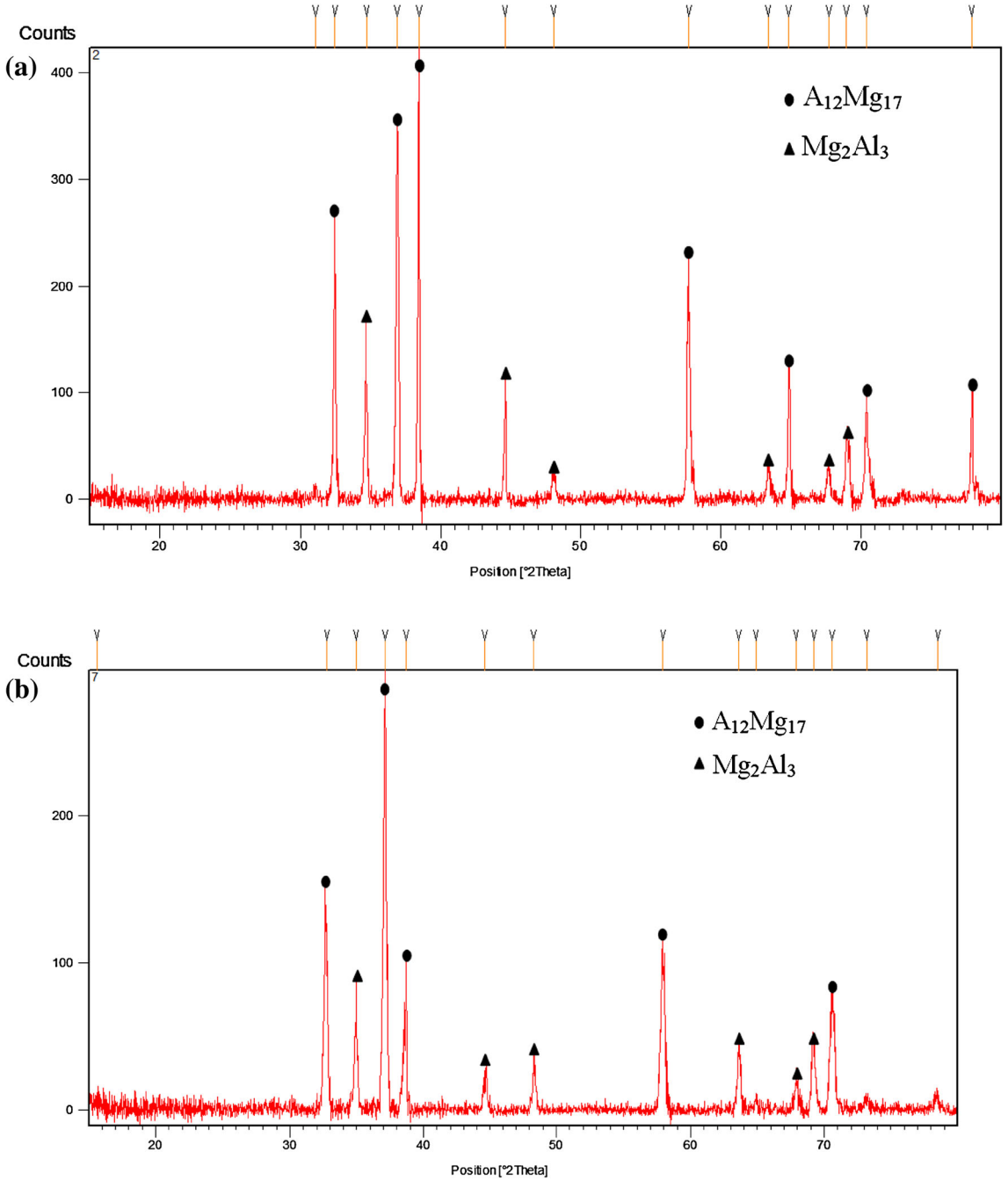

Fig. 6 XRD results of samples processed at **a** 1000 rpm—20 mm/min, **b** 1000 rpm—14 mm/min

ples. Figure 5a shows the EDX result of the corroded claded sample processed in combination 1, and Fig. 5b shows the EDX result of corroded claded sample processed in combination 8. The magnesium content in both the samples was corroded during the corrosion process, and among them, the sample processed in combination 8 showed more elimination of magnesium.

4.2 Effect of Process Parameters on the Microhardness of Claded Alloys

The intensity of precipitated intermetallics like $Al_{12}Mg_{17}$ and Mg_2Al_3 at the stir zone affected the microhardness of the claded materials. The friction stir processing tool had high contact time with the substrate and clad materials dur-

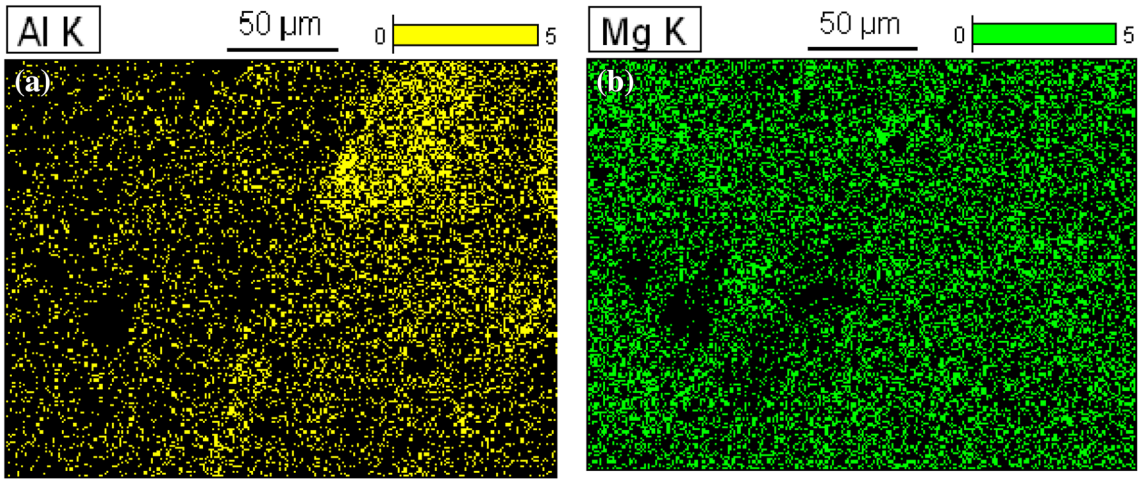

Fig. 7 Elemental mapping of Al/Mg processing cross section **a** Al elements on Mg side, **b** Mg elements on Al side

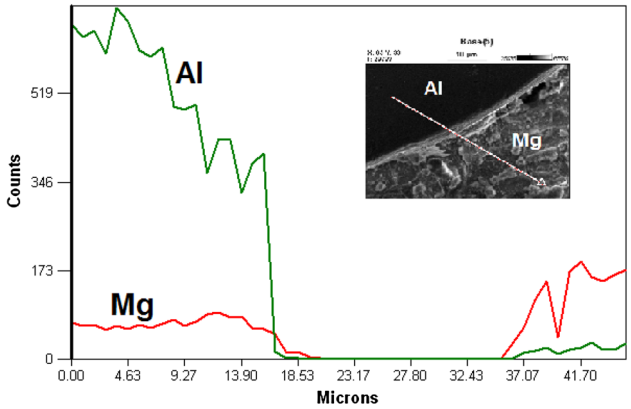

Fig. 8 EDS line scan data for Al/Mg-cladded cross section

ing low tool travel speed compared to the high tool travel speed. The friction between the rotating tool and the material induced heat generation at the processing zone, and the intensity of intermetallic particles increased with an increase in heat generation. However, for combination 7, heat generation was very intense compared to the other combinations. This intense heat generation resulted in the dissolution of the precipitated intermetallic particles again into the metal matrix, leading to the reduction in the intensity of intermetallics. Therefore, the sample processed in combination 7 recorded the lowest microhardness value. However, in the case of the samples processed in combination 8, intermetallics generated survived due to sufficient heat generation. Therefore, the comparatively high microhardness value was recorded for the combination 8. Figure 6a shows the results of XRD for combination 8. Figure 6a shows that the intensity of intermetallics was high at stir zone than the sample processed in combination 7.

4.3 Effect of Rotational Speed and Travel Speed on Tensile Strength Properties

The tensile properties of Al5086 aluminium cladded AZ31B magnesium plates showed a bimetallic tension behaviour. Individually, the tensile strength of Al5086 aluminium alloy is 304 MPa and that of AZ31B magnesium alloy is 250 MPa. However, the highest recorded tensile strength value of cladded samples was only 236 MPa (refer Table 4). The tensile strength properties of cladded samples were affected by bonding at the interface and the intensity of intermetallic particles along the joint line. Proper bonding at the interface of clad Al5086 alloy and substrate AZ31B magnesium alloy could not be achieved at high tool travel speeds. At high tool travel speed, the contact time of the tool with the materials was less. Therefore, achieving good bonding between the clad material and the substrate material was difficult. Moreover, the presence of intermetallic particles along the joint line induced brittleness between the joints. Figure 7 shows the elemental mapping at the cross-sectional area of the cladded sample. Figure 7 reveals that both Mg and Al elements were distributed on both sides of the joint interface and the EDS line analysis (refer Fig. 8) also supports this concept. The brittleness of the joints had increased with an increase in intensity of the intermetallic particles. The increase in rotational speed resulted in high-frictional heat input in the stir zone. Precipitation of intermetallic particles depended upon the intensity of heat input in the stir zone. Therefore, high heat input resulted in more precipitation of intermetallic particles along the joint line leading to poor tensile strength. Figure 9a shows the SEM of the fractured section of combination 8 sample, and Fig. 9b shows the SEM of the fractured section of combination 7 sample. SEM image of the fractured surface of combination 8 corresponding to the sample

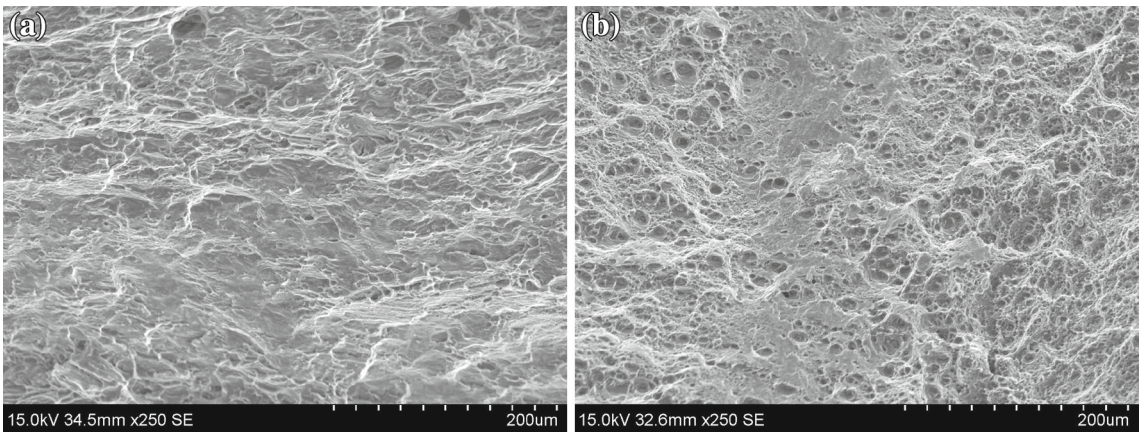

Fig. 9 SEM images of fractured surfaces of **a** 1000 rpm—20 mm/min, **b** 1000 rpm—14 mm/min samples

processed at high tool travel speed exhibited fewer ductile dimples and more cleavage facets conforming brittle-type fracture. Likewise, SEM image of the fractured surface of combination 7 corresponding to the sample processed at low tool travel speeds showed more ductile dimples because of the ductile failure.

5 Conclusion

In this research work, Al5086 aluminium alloy was cladded to the AZ31B magnesium alloy by friction stir processing technique. The following conclusions are derived from the study.

1. High corrosion rates were observed in the samples processed in high process parameter ranges. This is due to the presence of the higher percentage of magnesium traces on their surfaces.
2. The intensity of intermetallic particles in the stir zone determined the microhardness values of cladded alloys. Increasing the intensity of intermetallic particles in the stir zone has proportionally increased the microhardness values of the cladded samples.
3. The samples processed in higher rotational speeds have inferior tensile strengths due to the presence of intermetallics along the joint line.
4. Achievement of proper bonding between the clad material and the substrate material was difficult in high tool travel speeds due to less contact time between the tool and processing materials.

References

1. Aonuma, M.; Nakata, K.: Dissimilar metal joining of ZK60 magnesium alloy and titanium by friction stir processing. Mater. Sci. Eng. B **177**, 543–548 (2012)
2. Guo, H.X.; Ying, M.A.; Wang, J.S.; Wang, Y.S.; Dong, H.R.; Yuan, H.A.O.: Corrosion behavior of micro-arc oxidation coating on AZ91D magnesium alloy in NaCl solutions with different concentrations. Trans. Nonferrous Met. Soc. China. **22**, 1786–1793 (2012)
3. Lei, T.; Ouyang, C.; Tang, W.; Li, L.F.; Zhou, L.S.: Enhanced corrosion protection of MgO coatings on magnesium alloy deposited by an anodic electrodeposition process. Corros. Sci. **5**, 3504–3508 (2010)
4. Zhang, S.; Cao, F.; Chang, L.; Zheng, J.J.; Zhang, Z.; Zhang, J.; Cao, C.: Electrodeposition of high corrosion resistance Cu/Ni-P coating on AZ91D magnesium alloy. Appl. Surf. Sci. **257**, 9213–9220 (2011)
5. Tang, Y.; Zhao, X.; Jiang, K.; Chen, J.; Zuo, Y.: The influence of duty cycle on the bonding strength of AZ31B magnesium alloy microarc oxidation. Surf. Coat. Technol. **205**, 1789–1792 (2010)
6. Danisman, S.; Savas, S.: Relation between coating parameters and structural and mechanical properties of magnetron sputtered TiAlN coatings. Arab. J. Sci. Eng. **39**(06), 5025–5034 (2014)
7. Tosun, G.: Coating of AISI 1010 steel by Ni–WC using plasma transferred arc process. Arab. J. Sci. Eng. **39**(04), 3271–3277 (2014)
8. Tosun, G.: Ni–WC coating on AISI 1010 steel using TIG: microstructure and microhardness. Arab. J. Sci. Eng. **39**(03), 2097–2106 (2014)
9. Buytoz, S.; Orhan, A.; Gur, A.K.; Caligulu, U.: Microstructural development of Fe-Cr-C and B_4C powder alloy coating on stainless steel by plasma-transferred arc weld surfacing. Arab. J. Sci. Eng. **38**, 2197–2204 (2013)
10. Buytoz, S.; Ulutan, M.; Islak, S.; Kurt, B.; Celik, O.N.: Microstructural and wear characteristics of high velocity oxygen fuel (HVOF) sprayed NiCrBSi-SiC composite coating on SAE 1030 steel. Arab. J. Sci. Eng. **38**, 1481–1491 (2013)
11. Wu, G.; Zhang, X.; Zhao, Y.; Ibrahim, J.M.; Yuan, G.: Plasma modified Mg-Nd-Zn-Zr alloy with enhanced surface corrosion resistance. Corros. Sci. **78**, 121–129 (2014)
12. Hoche, H.; Rosenkranz, C.; Delp, A.; Lohrengel, M.M.; Broszeit, E.; Berger, C.: Investigation of the macroscopic and microscopic electrochemical corrosion behaviour of PVD-coated magnesium die cast alloy AZ91. Surf. Coat. Technol. **193**, 178–184 (2005)
13. Wu, G.; Dai, W.; Zheng, H.; Wang, A.: Improving wear resistance and corrosion resistance of AZ31 magnesium alloy by DLC/AlN/Al coating. Surf. Coat. Technol. **205**, 2067–2073 (2010)
14. Wang, X.; Zhu, L.; He, X.; Sun, F.: Effect of cerium additive on aluminum-based chemical conversion coating on AZ91D magnesium alloy. Appl. Surf. Sci. **280**, 467–473 (2010)

15. Wang, H.; Akid, R.; Gobara, M.: Scratch-resistance anticorrosion sol-gel coating for the protection of AZ31B magnesium alloy via a low temperature sol-gel route. Corros. Sci. **52**, 2565–2570 (2010)
16. Khramov, A.N.; Balbyshev, V.N.; Kasten, L.S.; Mantz, R.A.: Sol-gel coating with phosphonate functionalities for surface modification of magnesium alloys. Thin Solid Films **514**, 174–181 (2006)
17. Elsentriecy, H.H.; Luo, H.; Meyer, H.M.; Grado, L.L.; Qu, J.: Effects of pretreatment and process temperature of a conversion coating produced by an aprotic ammonium-phosphate ionic liquid on magnesium corrosion protection. Electrochim. Acta **123**, 58–65 (2014)
18. Lopez, A.J.; Torres, B.; Taltavull, C.; Rams, J.: Influence of high velocity oxygen fuel spraying parameters on the wear resistance Al-SiC composite coatings deposited on ZE41A magnesium alloy. Mater. Des. **43**, 144–152 (2013)
19. Chang, H.; Zheng, M.Y.; Xu, C.; Fan, G.D.; Brokmeier, H.G.; Wu, K.: Microstructure and mechanical properties of the Mg/Al multilayer fabricated by accumulative roll bonding (ARB) at ambient temperature. Mater. Sci. Eng. A **543**, 249–256 (2012)
20. Assidi, M.; Fourment, L.; Guerdoux, S.; Nelson, T.: Friction model for friction stir processing process simulation: calibrations from processing experiments. Int. J. Mach. Tools Manuf. **50**, 143–155 (2010)
21. Karam, A.; Mahmoud, T.S.; Zakaria, H.M.; Khalifa, T.A.: Friction stir welding of dissimilar A319 and A413 cast aluminum alloys. Arab. J. Sci. Eng. **39**, 6363–6373 (2014)
22. Krasnowski, K.: Experimental study of FSW T-joints of EN-AW6082-T6 and their behaviour under static loads. Arab. J. Sci. Eng. **39**, 9083–9092 (2014)